CONFIDENTIAL

Copy 349
RM L54J29a

NACA

RESEARCH MEMORANDUM

JET EFFECTS ON LONGITUDINAL TRIM OF AN AIRPLANE CONFIGURATION MEASURED AT MACH NUMBERS BETWEEN 1.2 AND 1.8

By Robert F. Peck

Langley Aeronautical Laboratory
Langley Field, Va.

CLASSIFIED DOCUMENT

This material contains information affecting the National Defense of the United States within the meaning of the espionage laws, Title 18, U.S.C., Secs. 793 and 794, the transmission or revelation of which in any manner to an unauthorized person is prohibited by law.

NATIONAL ADVISORY COMMITTEE FOR AERONAUTICS

WASHINGTON

January 18, 1955

CONFIDENTIAL

NATIONAL ADVISORY COMMITTEE FOR AERONAUTICS

RESEARCH MEMORANDUM

JET EFFECTS ON LONGITUDINAL TRIM OF AN AIRPLANE CONFIGURATION MEASURED AT MACH NUMBERS BETWEEN 1.2 AND 1.8

By Robert F. Peck

SUMMARY

An airplane model recently tested by the Pilotless Aircraft Research Division encountered large jet-induced effects on longitudinal trim at Mach numbers between 1.2 and 1.8. The delta-wing configuration tested had a relatively small horizontal tail mounted just behind and above the exit of a rocket nozzle. Jet effects are believed to have resulted from the fact that the horizontal tail either intersected or was very close behind a shock wave in the external flow originating near the intersection of the external flow and the jet boundary. The induced normal load at the tail was calculated to be approximately 10 percent of the static thrust of the rocket.

INTRODUCTION

Stabilizing and control surfaces have often been mounted downstream of propulsive jet exits. Recently, the Pilotless Aircraft Research Division tested a model which had a horizontal tail mounted just behind and above the exit of a rocket nozzle but outside of the rocket blast. The tests were conducted primarily to determine model-booster stability and separation characteristics, but records from the model flight (subsequent to model-booster separation) showed the presence of strong jet-induced effects on longitudinal trim.

Data are presented for Mach numbers between 1.2 and 1.8 and were obtained from tests conducted at the Langley Pilotless Aircraft Research Station at Wallops Island, Va.

SYMBOLS

C_m	pitching-moment coefficient, $\frac{I\ddot{\theta}}{qS\bar{c}}$
C_N	normal-force coefficient, $\frac{a_n}{g}\frac{W}{Sq}$
C_Y	side-force coefficient, $\frac{a_t}{g}\frac{W}{Sq}$
$\bar{c}$	wing mean aerodynamic chord, ft
g	acceleration due to gravity, ft/sec^2
I	moment of inertia in pitch, slug-ft^2
M	Mach number
N	normal force, lb
q	dynamic pressure, lb/sq ft
R	Reynolds number based on $\bar{c}$
S	wing area (including area enclosed within fuselage), sq ft
T_s	static thrust of rocket motor, lb
W	weight, lb
$\frac{a_n}{g}$	normal accelerometer reading
$\frac{a_t}{g}$	transverse accelerometer reading
$\ddot{\theta}$	pitching acceleration, radians/sec/sec

MODEL AND TESTS

A sketch and photographs of the model are shown in figures 1 and 2, respectively. This configuration has a fuselage of rather high fineness

ratio (equivalent fineness ratio = 15.2), a 55° modified delta wing, and sweptback horizontal and vertical tails. As shown in figures 1 and 2, the tails are mounted on a short boom which is above and extends behind the rocket-nozzle exit. This particular model has magnesium wings and tails and a wooden fuselage with a duralumin nose.

Before the sustainer rocket was fired, the model weight was 338.5 pounds; the moment of inertia in pitch was 118 slug-feet^2; and the center of gravity was located longitudinally at 0.20$\bar{c}$ and vertically at 2.7 inches above the rocket center line. After the sustainer-rocket burnout, the weight was 301.5 pounds; moment of inertia was 109.6 slug-feet^2; and the center of gravity was at 0.10$\bar{c}$ and 3.0 inches above the rocket center line. Variation of weight, moment of inertia, and center-of-gravity location were assumed to be linear with time during rocket burning (burning rate of rocket is approximately constant).

The ratio of total pressure to free-stream static pressure was approximately 100.0 throughout rocket burning, and the ratio of jet-exit static pressure to free-stream static pressure was approximately 4.4. The ratio of specific heats of the rocket gas was about 1.22, and the jet Mach number at the exit was approximately 2.6. As shown in figure 1, the half-angle of the nozzle divergence was 13°. A blast cone projected downstream was no closer than 3 inches (approximately 3/4 the jet-exit diameter) to the horizontal tail at any station.

Model instrumentation consisted of normal, longitudinal, and lateral accelerometers at the center of gravity and a normal accelerometer in the nose of the model. A radio telemeter, used to transmit information from these instruments, was mounted in the nose.

A double underslung booster with two 6-inch ABL Deacon rocket motors (fig. 2(b)) was used to propel the model to a Mach number of approximately 1.3. (The booster was also instrumented to provide more adequate information on separation.) After model-booster separation, the model coasted for a short interval (approximately 1 second) while decelerating to a Mach number of 1.2. Subsequently, the sustainer rocket fired and carried the model to a Mach number of about 1.8. Data were obtained while the rocket was thrusting and during coasting flight, both before and after rocket burning.

The CW Doppler velocimeter, NACA modified SCR 584 radar, and radiosonde were used to obtain free-stream conditions throughout the test.

Variation of the test Reynolds number with Mach number is shown in figure 3.

DATA REDUCTION

The dynamic-pressure data obtained from radar and radiosonde data were used to convert basic accelerometer readings into coefficient form.

$$C_N = \frac{a_n}{g}\frac{W}{Sq} \qquad C_Y = \frac{a_t}{g}\frac{W}{Sq}$$

The two normal accelerometers (one in nose and one at center of gravity) were used to measure the pitching acceleration $\ddot{\theta}$ which was used to calculate the total pitching-moment coefficient C_m.

$$C_m = \frac{I\ddot{\theta}}{qS\bar{c}}$$

Cross plots of C_m against C_N were used to obtain a measure of the stability during the parts of the flight that the model was oscillating.

Pitching moments, resulting from thrust misalinement (center of gravity always above the thrust line), were calculated by using preflight measurements of the vertical location of the center of gravity and the rocket-thrust characteristics.

RESULTS AND DISCUSSION

Time history.- A time history of the model flight before, during, and just after sustainer-rocket burning is shown in figure 4. Included in this history are the distance between the model and the booster in the early part of the flight (as obtained by integrating model and booster longitudinal accelerometers), Mach number, normal-force coefficient C_N, and side-force coefficient C_Y.

The plot of the distance between the model and the booster shows that the model is well ahead of the booster during the early part of the first oscillation. Zero value for this distance indicates that the entire model is ahead of the booster nose.

As evidenced in figure 4, the trim normal-force coefficient $C_{N_{trim}}$ was positive both before and after rocket burning but negative while the rocket was firing. This result, of course, was opposite to what would be expected from thrust moment effects alone because the model center of gravity was always above the thrust line. This effect will be discussed in detail later in the text.

The abrupt trim changes at model-booster separation, at rocket firing, and at rocket burnout resulted in the damped oscillations in pitch. At model-booster separation, the model was also disturbed in yaw. Oscillations in side-force coefficient C_Y were convergent, or damped, during coasting flight but of relatively constant amplitude during the first part of rocket burning (4.6 to 5.2 seconds) and divergent during the latter part of rocket burning (5.2 to 5.65 seconds). This indicates that, during rocket burning while trimmed at a negative C_N, the model had neutral to negative lateral dynamic stability. After 7.6 seconds, model motions were nonoscillatory (i.e., model was in trim).

Stability characteristics.- As mentioned previously, the pitching-moment coefficient C_m was measured by using the two normal accelerometers. In figure 5(a) the variations of C_m with normal-force coefficient C_N are shown as obtained during oscillations in pitch shown in figure 4. Although values of C_m were not corrected for damping, each plot obtained over $1\frac{1}{2}$ cycles of an oscillation showed no noticeable hysteresis (indicating low amount of rotary damping). Slopes measured from the data of figure 5(a) were used to obtain the stability parameter dC_m/dC_N shown in figure 5(b). Included in figure 5(b) is a theoretical estimate of dC_m/dC_N for the configuration as obtained from information given in reference 1.

Trim characteristics.- Basic measured trim data are shown in figure 6(a). Figure 6(b) shows the increments in trim $\Delta C_{N_{trim}}$ (center of gravity at $0.10\bar{c}$) due to total effects of rocket burning, due to thrust moment of the rocket, and due to jet-induced effects. The total increments in trim due to rocket burning were obtained by using changes in trim at rocket firing and at rocket burnout. Increments due to thrust moments were calculated by using rocket thrust, vertical location of the center of gravity, and stability information. It was then possible to obtain an estimate of the increment due to jet-induced effects. As shown in figure 6, the jet-induced effects are considerably greater than the total effects of rocket burning.

Tail loads.- The information shown in figures 5(b) and 6(b) was used to calculate jet-induced normal loads on the tail which were required to produce the trim changes. Estimated tail loads due to jet-induced effects are shown in figure 7. As shown in figure 7(a), the loads at the tail correspond to a C_N of the tail of roughly 0.3 (based on total true area of the tail). It is interesting to note that the ratio of normal force on the tail due to jet-induced effects ΔN_{tail} to the static thrust of the rocket T_s was approximately 0.1 as shown in figure 7(b).

Possible explanation of jet effects.- The information given in references 2 to 5 shows that an underexpanded propulsive jet issuing from the rear of a body at supersonic speeds may produce strong disturbances resulting in the formation of shock waves in the external flow. Data of references 5 and 6 further show that normal loads on surfaces intersecting or near these shocks may be of considerable magnitude. On the basis of information in these references, along with known rocket characteristics, it is believed the jet-induced effects resulted from conditions briefly described as follows:

Figure 8 is a simplified sketch illustrating what is believed representative of conditions in the vicinity of the tail. Jet flow issuing from the rocket-nozzle exit is underexpanded, and, as a result of this and of the fact that part of the flow is diverging along the nozzle walls, the jet initially continues to diverge after leaving the nozzle. As the jet boundaries increase, the jet may become overexpanded (i.e., jet static pressure below external-stream static pressure), tend to level off, and even tend to neck down slightly, farther downstream. When the external supersonic flow reaches the jet boundaries it must turn and a shock wave results. When and if this shock impinges on the tail surface, high positive normal loads result due to high positive pressures in the shock. When the tail is located close to and behind the shock, positive normal loads also result from flow angularity due to the external flow turning through the shock.

During the present test (i.e., between $M = 1.2$ and 1.8), it is probable that the tail, as illustrated, was either near (on downstream side) or intersected a shock wave originating in the region where external flow and the jet boundary came together. Information in reference 2 shows that the shock wave in the external flow may originate considerably ahead of the exit station (due to presence of boundary-layer air), and for this reason, the jet-induced effect measured in the present test may result almost entirely from external flow turning through the shock and towards the tail assembly, rather than from pressures in the shock itself. If the free-stream Mach number had reached a sufficiently high value, say, approximately $M = 3.0$, the tail would have been ahead of the shock wave and the jet-induced effect would have disappeared. Rather crude calculations, made by using two-dimensional flow equations, as well as the data of reference 6, verify the foregoing explanation.

Even though airplanes in current use have different exhaust conditions (i.e., generally lower pressure ratios and sonic rather than supersonic jets), it is probable that aircraft with engines in present-day use might encounter a like condition at supersonic speeds, at least when the ratio of jet static pressure to free-stream static pressure is sufficiently high to cause appreciable jet divergence. It is very likely that the power plants of the rocket, or similar power plants which may be used in the future, would produce similar effects unless all surfaces are kept ahead of the jet exit.

Lateral stability.- Estimates of the lateral-stability boundary of this configuration were made (by methods given in ref. 7) by using data presented in reference 1 (corrected for differences in tail configuration), along with measured inertias and estimated inclination of the principal axis. These estimates indicated that dynamic instability could very well exist when the model was trimmed at negative lifts due to negative inclinations of the principal axis. As a result of these calculations, it is believed the dynamic instability (indicated on fig. 4 to be between 5.2 and 5.65 seconds) was not caused directly by the jet but by the fact that the model was trimmed at lifts below the lateral-stability boundary.

CONCLUDING REMARKS

During the flight test of a delta-wing airplane configuration having a relatively small horizontal tail mounted just behind and above a propulsive jet exit, strong jet effects on longitudinal trim were measured at Mach numbers between 1.2 and 1.8. It is believed that these jet-induced effects resulted primarily from influences on the horizontal tail of a shock wave (in the external flow) originating at the intersection of the external flow and the jet boundary.

Langley Aeronautical Laboratory,
National Advisory Committee for Aeronautics,
Langley Field, Va., October 15, 1954.

REFERENCES

1. Margolis, Kenneth, and Bobbitt, Percy J.: Theoretical Calculations of the Stability Derivatives at Supersonic Speeds for a High-Speed Airplane Configuration. NACA RM L53G17, 1953.

2. Englert, Gerald W., Vargo, Donald J., and Cubbison, Robert W.: Effect of Jet-Nozzle-Expansion Ratio on Drag of Parabolic Afterbodies. NACA RM E54B12, 1954.

3. Cortright, Edgard M., Jr., and Schroeder, Albert H.: Investigation at Mach Number 1.91 of Side and Base Pressure Distributions Over Conical Boattails Without and With Jet Flow Issuing From Base. NACA RM E51F26, 1951.

4. Cortright, Edgard M., Jr., and Kochendorfer, Fred D.: Jet Effects on Flow Over Afterbodies in Supersonic Stream. NACA RM E53H25, 1953.

5. Hatch, John E., Jr., and Savelle, William M.: Some Effects of a Sonic Jet Exhaust on the Loading Over a Yawed Fin at a Mach Number of 3.03. NACA RM L52L02a, 1953.

6. Bressette, Walter E.: Investigation of the Jet Effects on a Flat Surface Downstream of the Exit of a Simulated Turbojet Nacelle at a Free-Stream Mach Number of 2.02. NACA RM L54E05a, 1954.

7. Campbell, John P., and McKinney, Marion O.: Summary of Methods for Calculating Dynamic Lateral Stability and Response and for Estimating Lateral Stability Derivatives. NACA Rep. 1098, 1952. (Supersedes NACA TN 2409.)

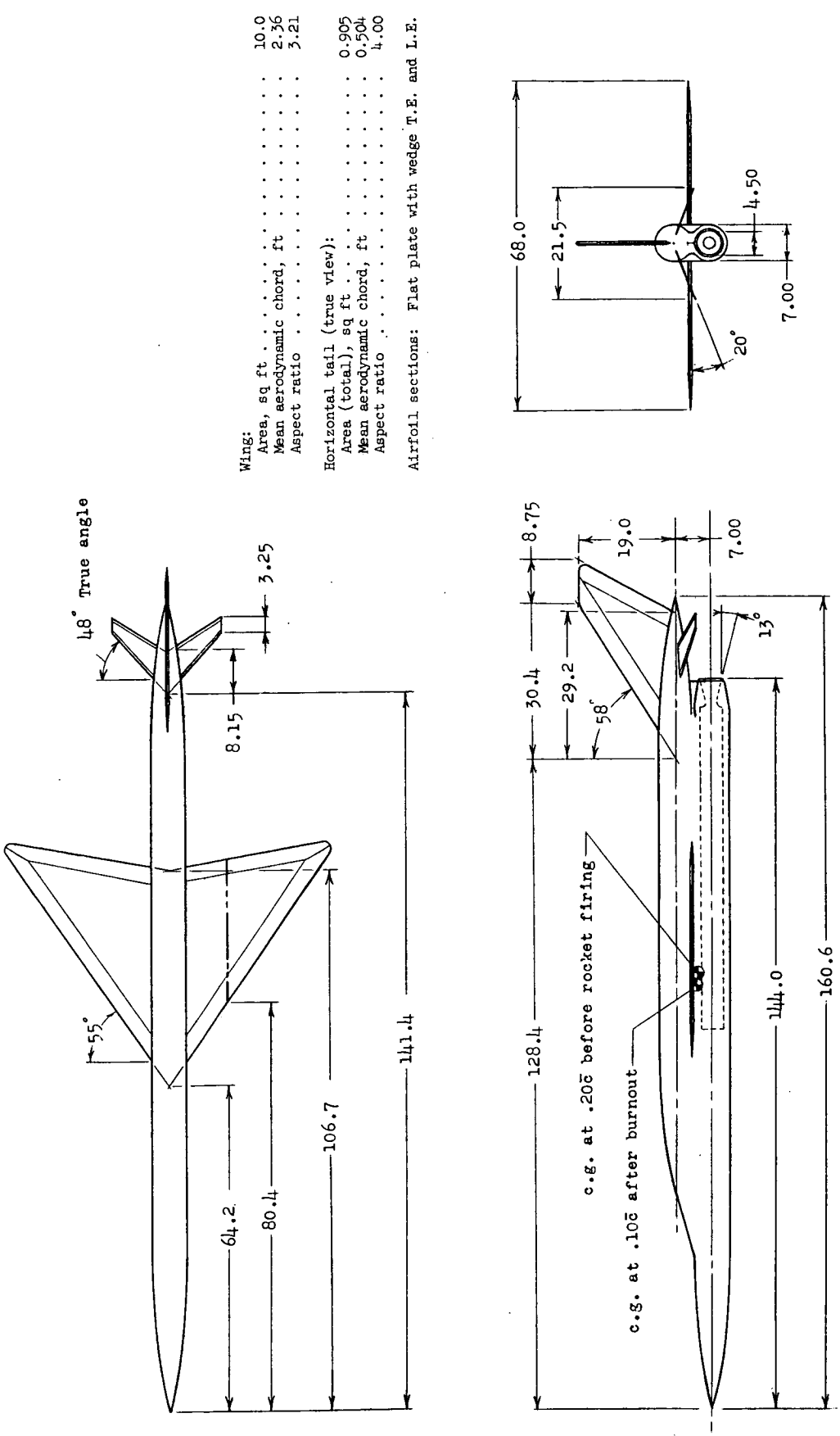

Figure 1.- Sketch of test configuration. All dimensions are in inches.

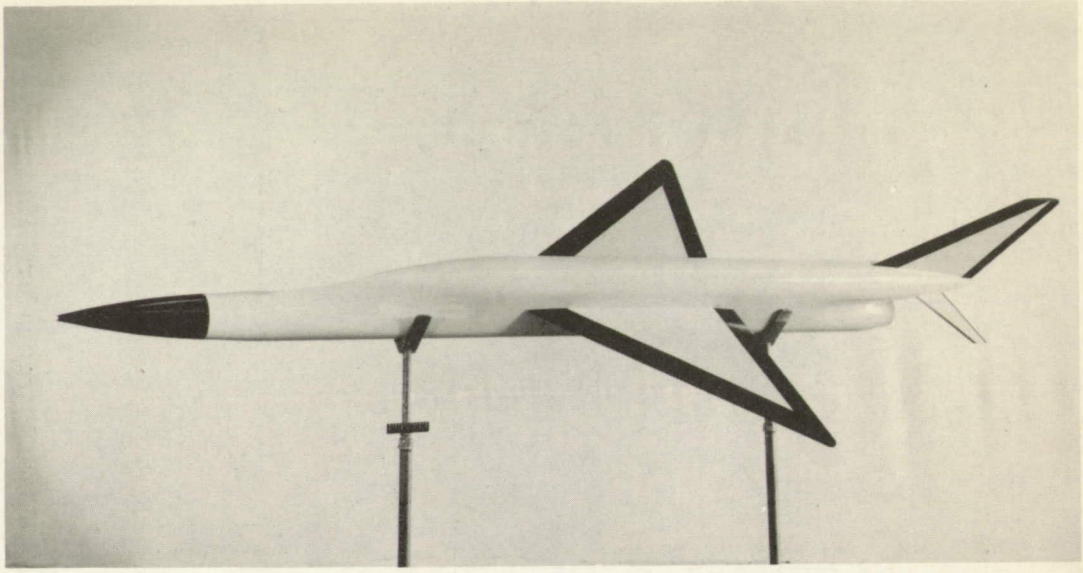

L-81152.1

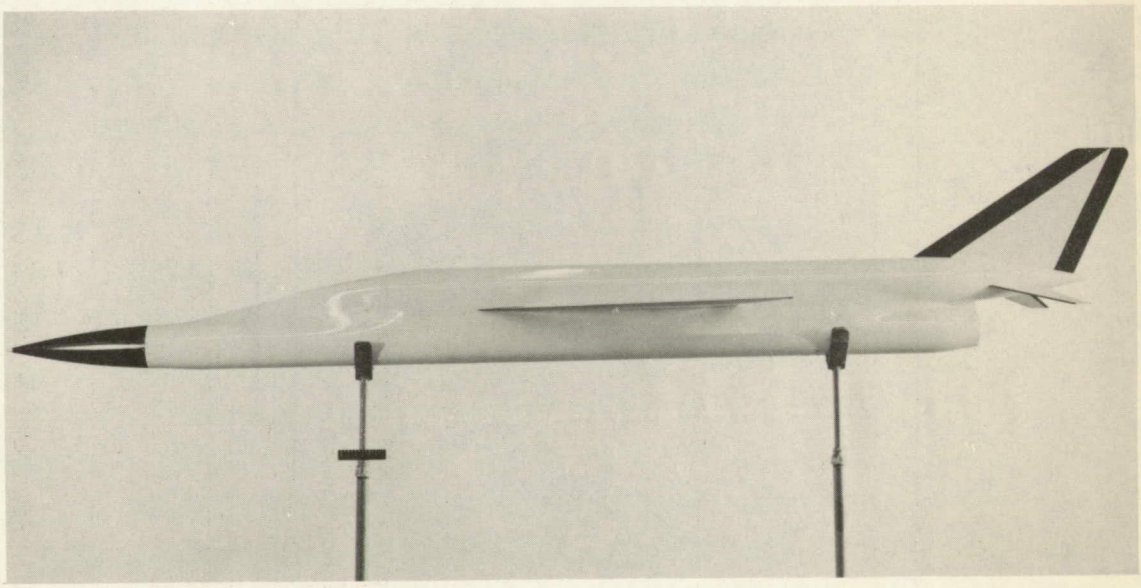

L-81151.1

(a) Model.

Figure 2.- Model and model-booster combination.

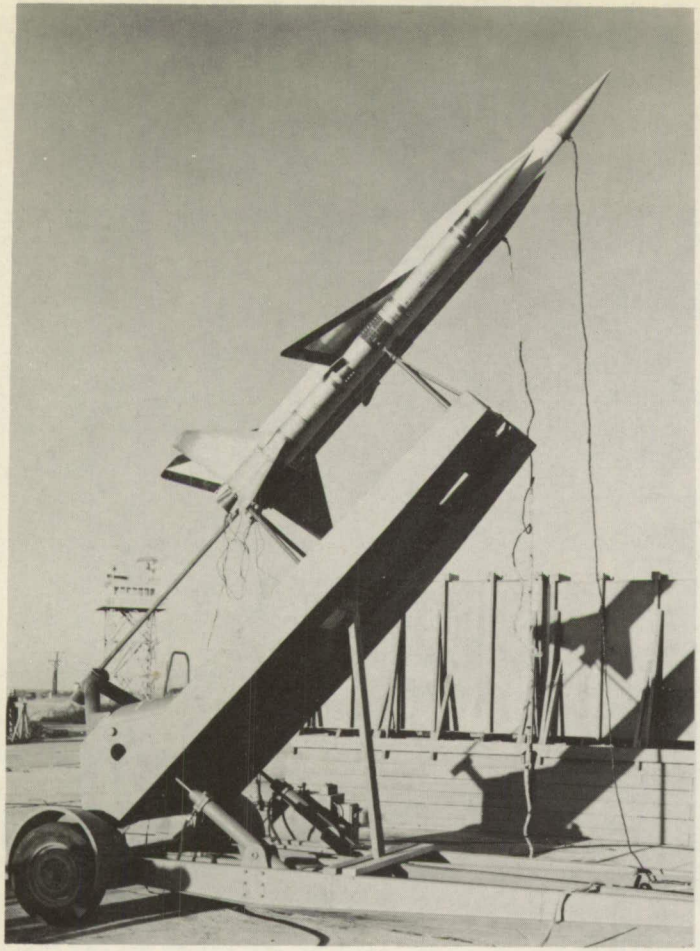

L-82845

L-82844

(b) Model-booster combination on launcher.

Figure 2.- Concluded.

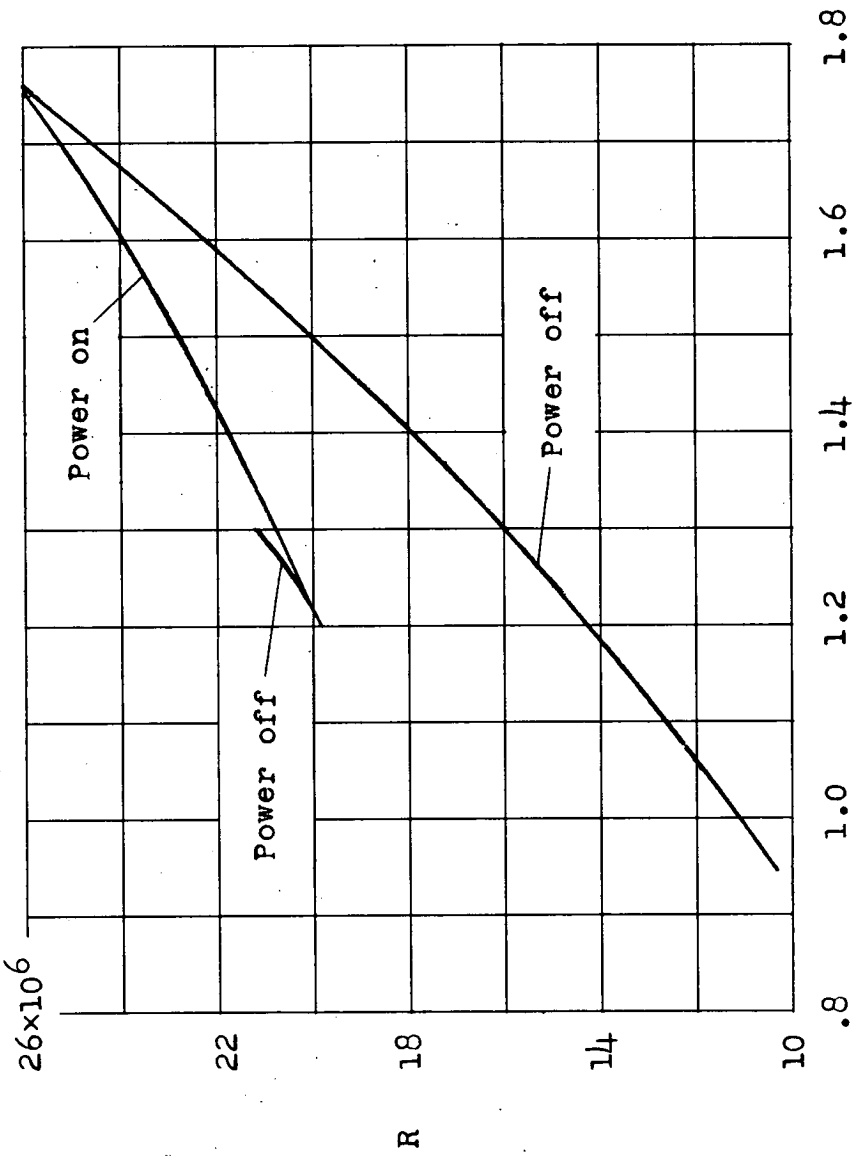

Figure 3.- Variation of test Reynolds number (based on $\bar{c}$) with Mach number.

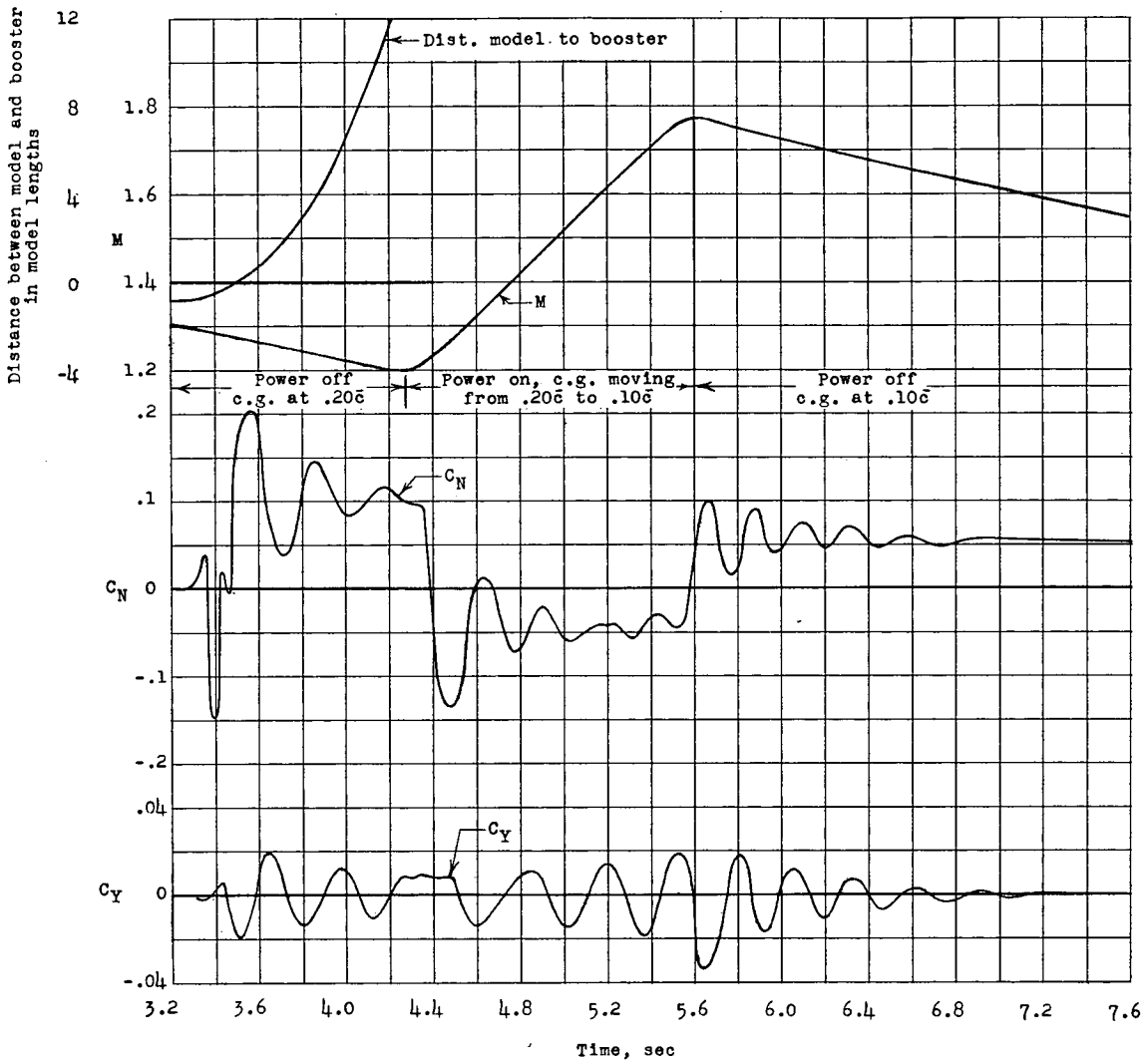

Figure 4.- Time history of part of flight during which model motions were oscillatory.

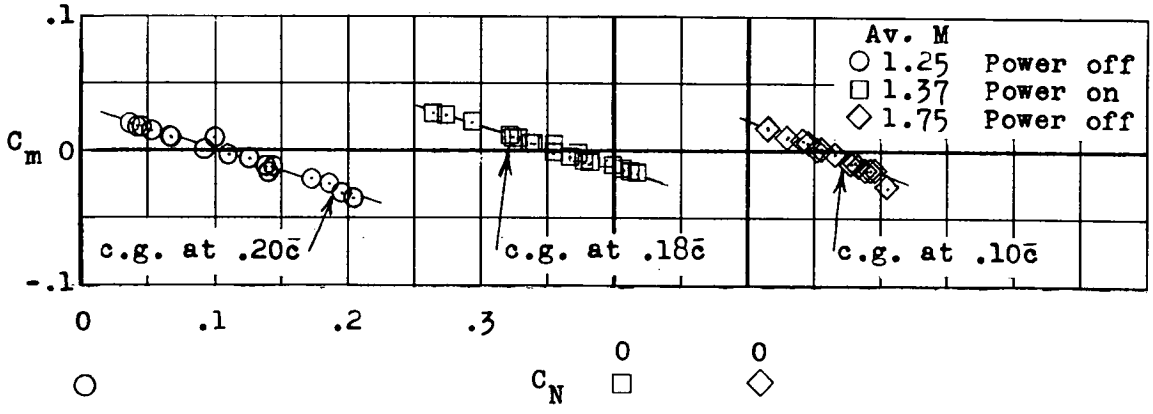

(a) Variation of pitching-moment coefficient with normal-force coefficient.

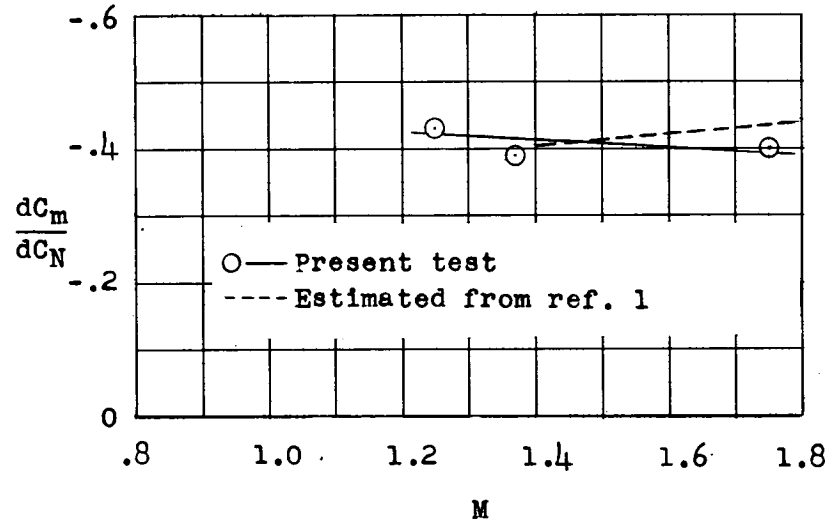

(b) Variation of stability parameter dC_m/dC_N with Mach number for center of gravity at 0.10c̄.

Figure 5.- Longitudinal-stability characteristics determined by using two normal accelerometers.

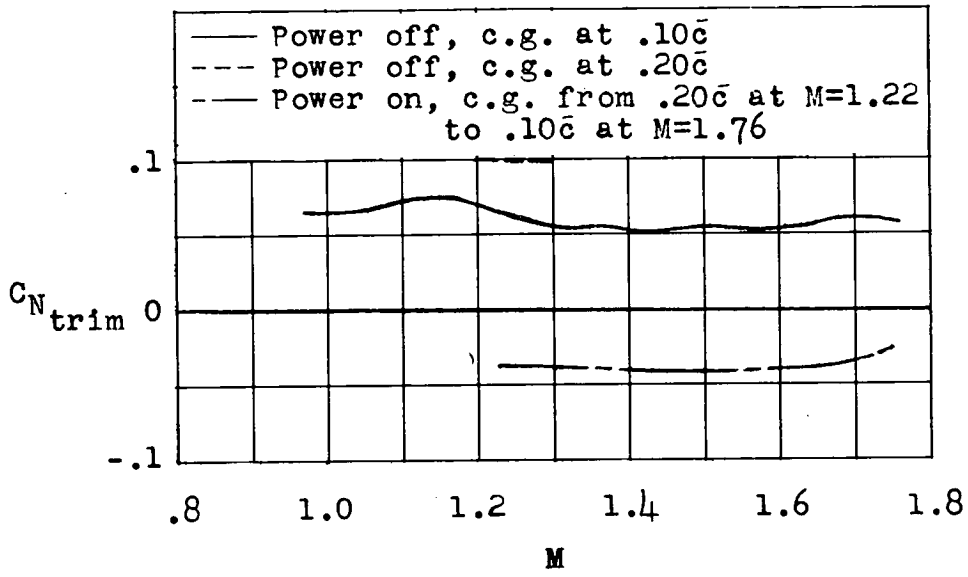

(a) Basic measured trim data.

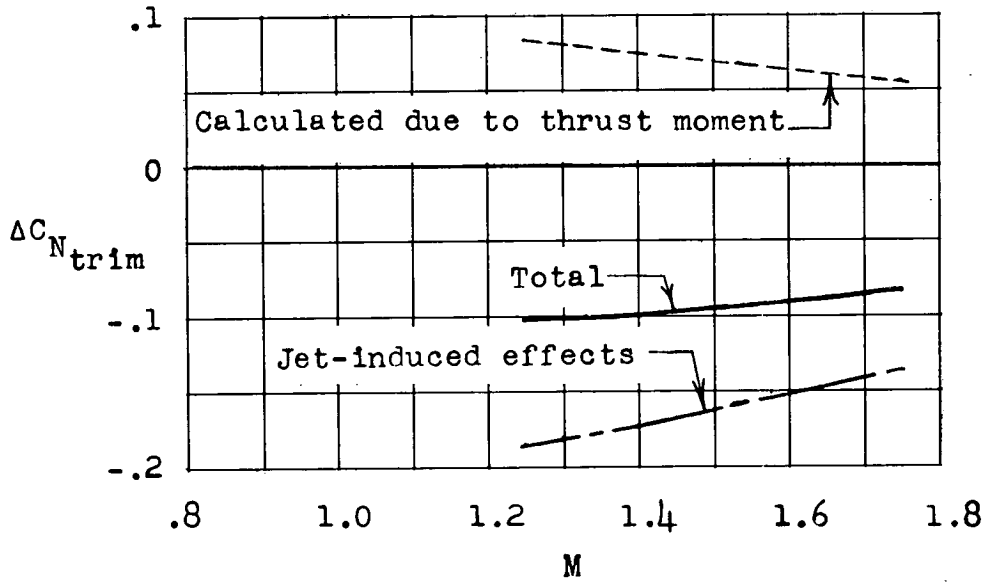

(b) Increments in $C_{N_{trim}}$ due to power effects with center of gravity at 0.10c̄.

Figure 6.- Trim characteristics of test configuration.

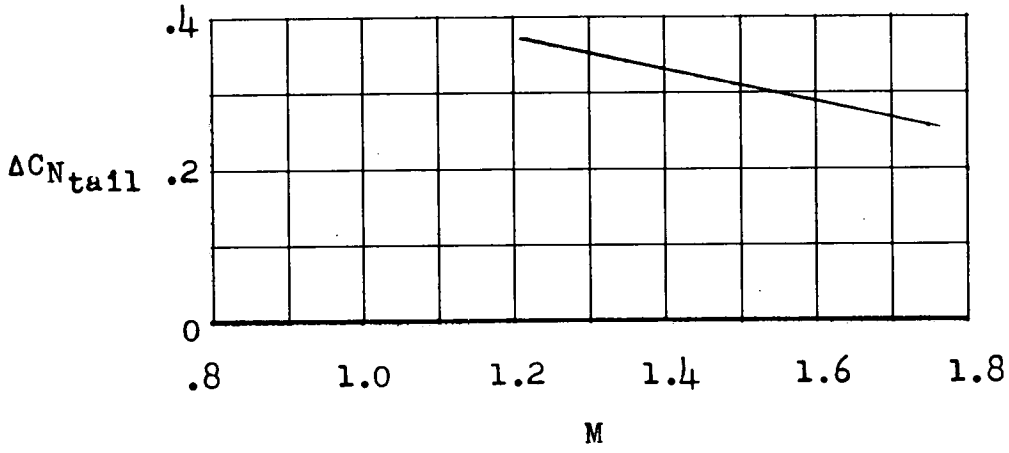

(a) Estimated increment in C_N of tail based on tail area.

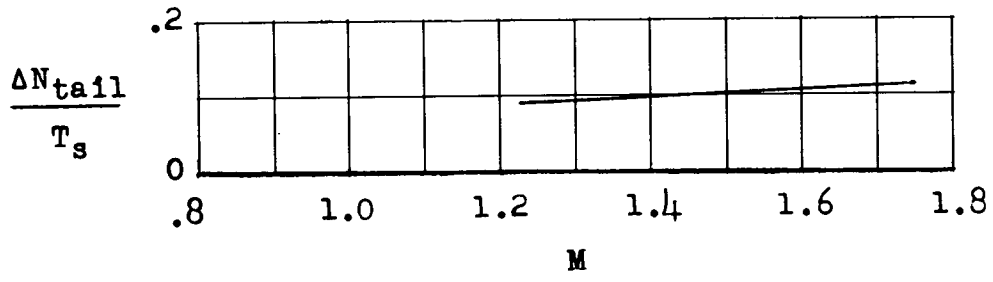

(b) Ratio of estimated normal-force increment on tail over static thrust of rocket.

Figure 7.- Estimated tail loads due to jet-induced effects necessary to produce measured trim changes.

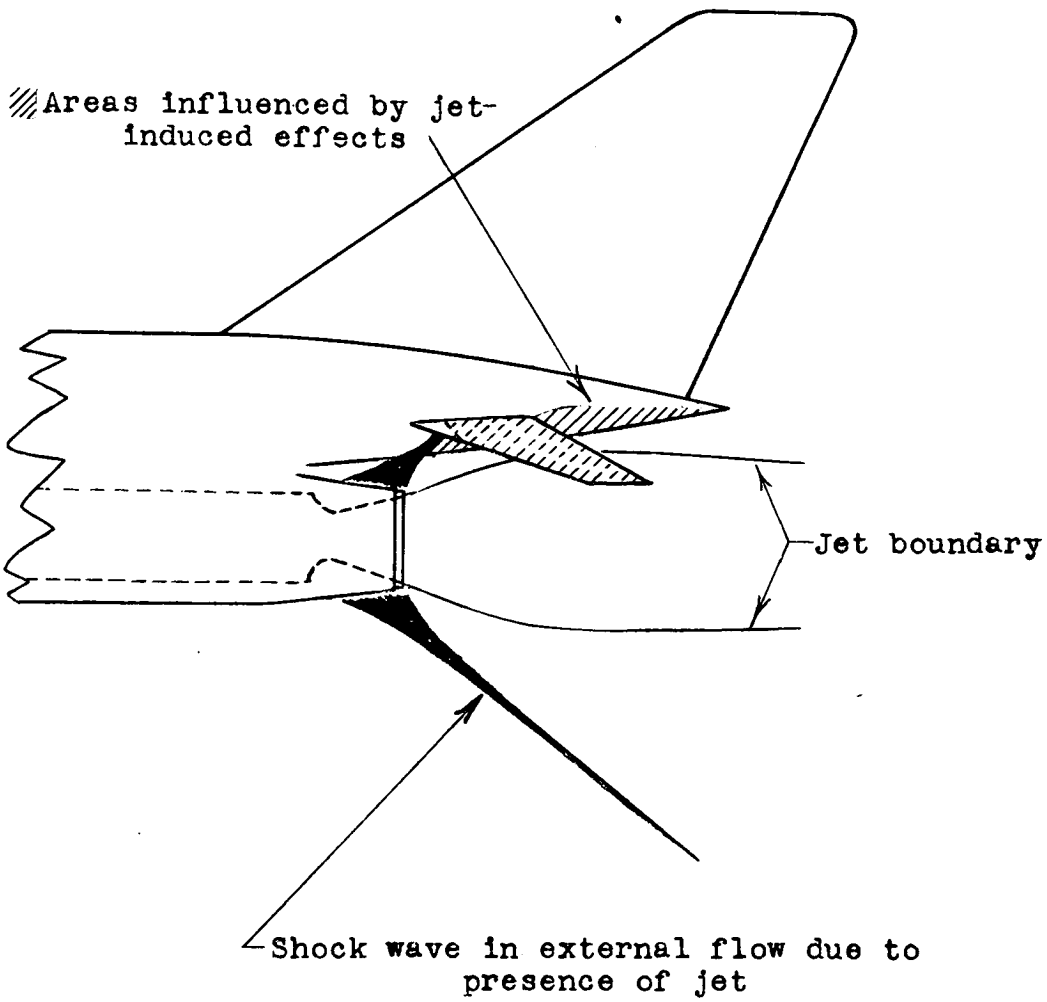

Figure 8.- Simplified sketch illustrating possible explanation of jet-induced effects at supersonic speeds.